PAPER • **OPEN ACCESS**

Modelling and experimental evidence of the cathode erosion in a plasma spray torch

To cite this article: M Baeva *et al* 2022 *J. Phys. D: Appl. Phys.* **55** 365202

OPEN ACCESS
IOP Publishing
Journal of Physics D: Applied Physics
J. Phys. D: Appl. Phys. **55** (2022) 365202 (13pp)
https://doi.org/10.1088/1361-6463/ac791c

Modelling and experimental evidence of the cathode erosion in a plasma spray torch

M Baeva[1,*], M S Benilov[2,3], T Zhu[1], H Testrich[1], T Kewitz[1] and R Foest[1]

[1] Leibniz Institute for Plasma Science and Technology, Felix-Hausdorff-Str. 2, 17489 Greifswald, Germany
[2] Departamento de Física, Faculdade de Ciências Exatas e da Engenharia, Universidade da Madeira, Largo do Município, 9000 Funchal, Portugal
[3] Instituto de Plasmas e Fusão Nuclear, Instituto Superior Técnico, Universidade de Lisboa, 1041 Lisboa, Portugal

E-mail: baeva@inp-greifswald.de

Received 2 May 2022, revised 31 May 2022
Accepted for publication 15 June 2022
Published 24 June 2022

Abstract

The lifetime of tungsten cathodes used in plasma spray torches is limited by processes leading to a loss of cathode material. It was reported in the literature that the mechanism of their erosion is the evaporation. A model of the ionization layer of a cathode is developed to study the diffusive transport of evaporated tungsten atoms and tungsten ions produced due to ionization by electron impact in a background argon plasma. It is shown that the Stefan–Maxwell equations do not reduce to Fick law as one could expect for the transport of diluted species, which is due to significant diffusion velocities of argon ions. The ionization of tungsten atoms occurs in a distance of a few micrometers from the cathode surface and leads to a strong sink, which increases the net flux of tungsten atoms far beyond that obtained in absence of tungsten ions. This shows that the tungsten ions are driven by the electric field towards the cathode resulting in no net diffusive flux and no removal of tungsten species from the ionization layer even if convection is accounted for. A possible mechanism of removal is found by extending the model to comprise an anode. The extended model resolves the inter-electrode region and provides the plasma parameters for a current density corresponding to the value at the center of the cathode under typical arc currents of 600 A and 800 A. The presence of the anode causes a reversal of the electric field on the anode side, which pulls the ions away from the ionization layer of the cathode. The net flux of tungsten ions can be further fortified by convection. This model allows one to evaluate the loss of cathode material under realistic operating conditions in a quantitative agreement with measured values.

Keywords: plasma spray torch, erosion, tungsten cathode, ionization layer, evaporation, field reversal, convection

(Some figures may appear in colour only in the online journal)

* Author to whom any correspondence should be addressed.

1. Introduction

The lifetime of the cathode in plasma spray torches is limited by the process of erosion. The evaporation of atoms has been considered as the major mechanism of erosion of refractory cathodes applied in free-burning arcs under normal operation conditions [1]. The cathodes used in plasma spray torches typically include doping materials (e.g. ThO_2, LaO_2, CeO_2) that lower the work function of the material and allow electron emission at temperatures below that in case of pure tungsten. The evaporation of the additives can lead to a local lack of additives followed by an increase of the temperature, which in turn results in an increase of the evaporation [2, 3]. On the other hand, the evaporated atoms can undergo backscattering in the background plasma and return to the cathode [4]. Evaporated atoms can become ionized and return as ions to the cathode [1]. These processes, therefore, reduce the flux of evaporated atoms (J_{vap}) compared to the value given by the Langmuir equation

$$J_{vap} = \frac{p_v}{\sqrt{2\pi m_w k_B T_c}}, \quad (1)$$

where p_v, m_w and T_c denote the equilibrium vapour pressure, the particle mass of the cathode material, and the temperature at the cathode surface, respectively. k_B is the Boltzmann constant.

Considerations of evaporated metal atoms have been previously reported. Nemchinsky [1] proposed a model to estimate the fraction of evaporated atoms not returning to the cathode (the escape factor) in a free-burning arc. According to this model, the tungsten atoms are instantly ionized and diffuse in a quasi-neutral plasma, in which the temperatures of electrons and heavy particles are equal. This implies that the evaporated atoms reach the core of the arc plasma being in the state of a local thermodynamic equilibrium.

The net flux of vapor from a solid surface in an ambient gas was analyzed by Benilov *et al* [4] with account of backscattering of the vaporized atoms. It was shown that if the equilibrium vapor pressure is lower than the ambient pressure, the removal of the vapor from the surface is due to diffusion into the bulk of the gas. As a consequence, the net flux of the vapor from the surface is much smaller than the Langmuir value. If the equilibrium vapor pressure exceeds the ambient pressure, a flow of the vapor from the surface appears and the net flux is comparable to the Langmuir value.

In contrast to [1], Ortega *et al* [5] consider the diffusion of tungsten atoms and ions in the non-equilibrium ionization layer of an arc plasma in argon at atmospheric pressure, where constant but different values of the temperatures of electrons and heavy particles (argon atoms and ions) are assumed. The argon plasma was the background, in which the diffusion of tungsten atoms and ions was considered. The particle densities of the background were determined according to the model of the ionization layer proposed by Almeida *et al* [6]. The model by Ortega *et al* was primarily focused on the behaviour of the evaporated cathode material and did not provide any estimate concerning the cathode erosion. This is probably related to the boundary condition set for tungsten atoms, which imposes a net flux of tungsten atoms tending to zero.

In this work, the question of evaluation of the net flux of metal vapor from the cathode into a high-pressure arc, or, equivalently, of the mass loss of thermionic cathodes is revisited with the use of numerical modelling. The transport of tungsten atoms and ions in an atmospheric-pressure argon plasma is considered as a typical example. The conclusion of the work [4] that the removal of the vapor from the surface is due to diffusion into the bulk of the gas and, therefore, the erosion rate is much smaller than the Langmuir value, is confirmed. Moreover, it is shown that the steady-state cathode erosion rate is zero if the computation domain includes only the near-cathode region bordering the equilibrium arc column, and non-zero erosion rate is obtained if the plasma region near an absorbing anode is included in the calculation domain. This result has a clear physical meaning: the steady-state cathode erosion rate is affected by the process of removal of tungsten from the arc occurring at an absorbing anode (or, in other cases, at absorbing walls), even if this process occurs far away from the cathode.

The paper is organized as follows. Experimental findings concerning the operation of the torch are given in section 2. The modelling of the transport of tungsten atoms and ions in the ionization layer on the cathode side is presented in section 3. In section 4, the transport of tungsten atoms and ions is treated in the framework of the unified microarc model. Results are given and discussed in section 5. Final remarks and conclusions are summarized in section 6. Cross section data and rate coefficients, data needed to compute binary diffusion coefficients as well as some details on the equations are given in the appendix.

2. Experimental findings

The commercial device Oerlikon Metco F4MB-XL [7] has been considered in studies related to deposition applications [8]. The torch arrangement (figure 1) includes a cathode (WL10) by Plansee made of lantanated tungsten [9] attached to a copper holder. The cylindrical part of the cathode has a radius of 4.9 mm. The conical tip has a length of 10.6 mm and it is rounded with a radius of 2 mm. A cylindrically symmetric nozzle serves as anode. The torch is typically operated in pure argon, and mixtures of argon with hydrogen or nitrogen with flow rates between 40 and 80 NLPM and direct electric current of several hundred amperes.

The cathode is eroding during the operation. Its tip is exposed to temperatures above 3000 K, which are needed for the emission of electrons and the sustainment of the arc discharge. Figure 2 shows images in side and frontal views of a fresh cathode and the same cathode after 6 and 12 h of operation. Evaporation of cathode material occurs and the mass of the cathode is reduced. Figure 3 shows that the loss of mass amounts to several milligrams after 6 and 12 h of operation at a current of 600 A. At a current of 800 A and 6 h of operation the mass loss is more than 10 mg. While the rate of mass loss is almost constant at the current value of 600 A,

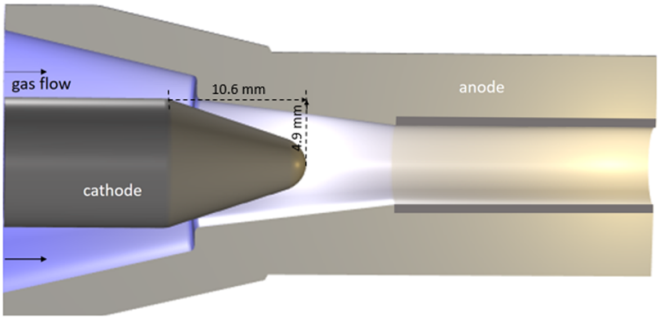

Figure 1. Schematics of the torch head.

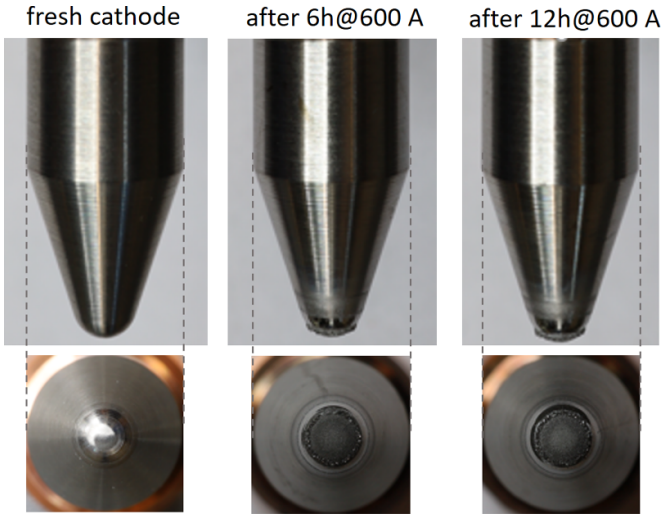

Figure 2. Images of the cathode before and after operation of 6 and 12 h.

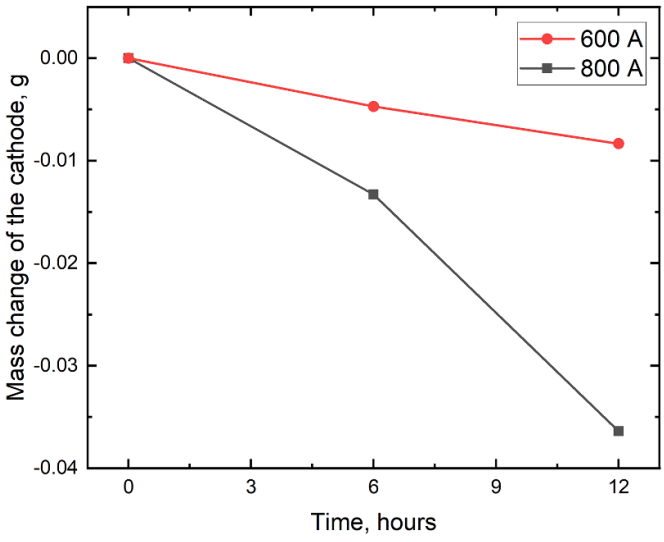

Figure 3. The mass change of the cathode during operation for arc currents of 600 A and 800 A.

it tends to increase at the current value of 800 A so that the mass loss becomes about 36 mg after 12 h of operation. In average, a mass loss of respectively (0.7–0.8) mg at 600 A and (2.2–3.1) mg at 800 A per 1 h of operation is measured.

3. Transport of tungsten species in the ionization layer of the cathode

In the previous work [8], a model of the cathode and its boundary layer has been considered as a part of the combined model of the plasma spray torch. The temperatures of the electrons and the heavy particles in the argon plasma have been obtained along with the distribution of the normal current density and the surface temperature of the cathode. The species' temperatures have the meaning of average temperatures in the ionization layer of the cathode, which is spatially unresolved.

In the present work, a one-dimensional model of the ionization layer is employed to obtain the number densities of the argon species for given species temperatures and electric current density. The argon plasma is then the background, in which tungsten atoms are released from the cathode and undergo ionization. A sketch to the formulation of the model is given in figure 4.

3.1. Model of the ionization layer

The model of the ionization layer of the cathode is based on the description in [6]. It is one-dimensional in direction perpendicular to the cathode surface due to the small thickness of the near-cathode region. The origin of the x-axis ($x = 0$) is on the cathode wall asymptotically setting the thickness of the space charge sheath to zero. In the ionization layer, a quasi-neutral plasma at constant pressure (1 atm) is considered that contains electrons, atoms and singly charged ions of argon. The heavy particles (atoms and ions) are characterized by a common temperature (T_h), while the electrons are characterized by a temperature T_e. T_h and T_e are assumed constant across the layer. The contribution of multiply charged ions becomes important for temperatures beyond about 25 000 K [6], which is not reached under typical operating conditions of the plasma spray torch (see figure 5(c) below and the results from the magnetohydrodynamic model in [8]). Convective transport is initially neglected but can be included for the sake of the study as shown below. Electron impact ionization of argon atoms and recombination in three-body collisions with an electron as the third body are taken into account. The rates of production and loss of charged particles are unequal due to the diffusive and drift transport to the cathode surface. The length L of the layer is chosen large enough so that the values of number densities of electrons and ions obey ionization equilibrium.

The equation of species' conservation is written as

$$\frac{d}{dx}(J_\mathrm{k}) = \omega_\mathrm{k}, \tag{2}$$

where $J_\mathrm{k} = n_\mathrm{k} v_\mathrm{k}$ is the flux density of species of kind 'k' with number densities n_k and mean velocities v_k, and a net rate of production ω_k. The corresponding rates are related to each other, i.e.

$$\omega_\mathrm{i} = \omega_\mathrm{e} = -\omega_\mathrm{a} = K_\mathrm{i} n_\mathrm{a} n_\mathrm{e} - K_\mathrm{r} n_\mathrm{i} n_\mathrm{e}^2, \tag{3}$$

with K_i and K_r being the rate coefficients for ionization and recombination, respectively. In equation (3), the indices i, e,

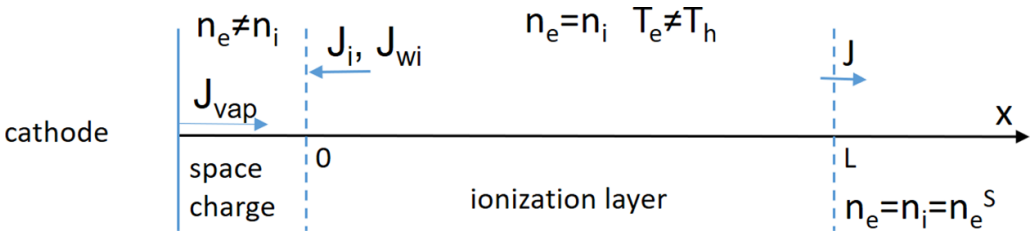

Figure 4. A sketch to the model formulation.

and a refer to ions, electrons, and atoms, respectively. It follows from equations (2) and (3) that

$$\frac{d}{dx}(J_\mathrm{i}+J_\mathrm{a})=0, \tag{4}$$

$$\frac{d}{dx}(J_\mathrm{i}-J_\mathrm{e})=0. \tag{5}$$

From the conservation of nuclei equation (4), it follows $J_\mathrm{i}+J_\mathrm{a}=\mathrm{const}$. Since there is no accumulation or release of argon nuclei on the electrode boundary, the constant value is equal to zero everywhere, i.e. $J_\mathrm{i}+J_\mathrm{a}=0$. The density of electric current is expressed as $j/e=J_\mathrm{i}-J_\mathrm{e}=J$ so that equation (5) represents the equation of current continuity.

The transport of plasma species for the case of constant temperature and pressure may be written as [10]

$$-k_\mathrm{B}T_\mathrm{k}\frac{dn_\mathrm{k}}{dx}+eZ_\mathrm{k}n_\mathrm{k}E-\sum_{l=i,e,a}\frac{n_\mathrm{k}n_l k_\mathrm{B}T_\mathrm{kl}C_\mathrm{kl}}{nD_\mathrm{kl}}(v_\mathrm{k}-v_l)=0, \tag{6}$$

where D_kl are the binary diffusion coefficients (see appendix below), T_kl are the reduced temperatures, Z_k take values of 0 ($k=a$), 1 ($k=i$), and -1 ($k=e$), E is the electric field strength, C_kl are correction factors, $n=\sum_k n_\mathrm{k}$ is the total number density. Further relations follow from the assumption of quasi-neutrality $n_\mathrm{e}=n_\mathrm{i}$ and the Dalton law for the total pressure $p=(n_\mathrm{a}+n_\mathrm{i})k_\mathrm{B}T_\mathrm{h}+n_\mathrm{e}k_\mathrm{B}T_\mathrm{e}$, which is a given parameter.

Writing down the equations for ions and electrons according to equation (6) and summing them up, one gets an equation for n_i.

$$\frac{dn_\mathrm{i}}{dx}=-\frac{T_\mathrm{h}}{T_\mathrm{h}+T_\mathrm{e}}(n_\mathrm{a}+n_\mathrm{i})\left[\frac{C_{ia}}{nD_{ia}}+\frac{T_\mathrm{e}}{T_\mathrm{h}}\frac{C_{ea}}{nD_{ea}}\right]J_\mathrm{i}+n_\mathrm{a}\frac{T_\mathrm{e}}{T_\mathrm{h}+T_\mathrm{e}}\frac{C_\mathrm{ea}}{nD_\mathrm{ea}}\frac{j}{e}. \tag{7}$$

Expressing now J_i from equation (7) and replacing it in equation (2), the equation becomes

$$\frac{d}{dx}\left(-c\frac{dn_\mathrm{i}}{dx}+\gamma\right)=f, \tag{8}$$

where $-c=1/A$, $\gamma=-B/A$ with A and B denoting respectively the multiplier and the last term in equation (7), and $f=\omega_\mathrm{i}$.

A dimensionless number density is introduced as $\hat{n}_\mathrm{i}=n_\mathrm{i}/n_\mathrm{i}^S$, where n_i^S is the equilibrium value. The boundary conditions to the equation for $\hat{n}_i$ are set as

$$\hat{n}_\mathrm{i}=\begin{cases}0, & \text{for } x=0\\ 1, & \text{for } x=L\end{cases}. \tag{9}$$

The equation is solved for given values of the total pressure p, temperatures of heavy particles, T_h, and electrons, T_e, and the current density j. The electron number density n_e equals n_i due to the condition of quasi-neutrality and is then also obtained.

The strength of the electric field E is expressed in terms of $\frac{dn_\mathrm{i}}{dx}$, J_i, and n_i as follows

$$E=\frac{k_\mathrm{B}T_\mathrm{h}}{en_\mathrm{i}}\frac{dn_\mathrm{i}}{dx}+(n_\mathrm{a}+n_\mathrm{i})\frac{k_\mathrm{B}T_\mathrm{h}C_\mathrm{ia}}{en_\mathrm{i}nD_\mathrm{ia}}J_\mathrm{i}+\frac{k_\mathrm{B}T_\mathrm{e}C_\mathrm{ie}}{enD_\mathrm{ie}}. \tag{10}$$

3.2. Transport of tungsten atoms and ions in the model of the ionization layer

The argon plasma in the ionization layer is considered as a background into which the tungsten atoms are released from the cathode. The tungsten particles are assumed to not influence the properties of the background plasma since their number density is expected to be much lower than that of the argon species. Ionization and recombination processes leading to a production and a loss of tungsten ions are taken into account. The rate of net production of tungsten ions, ω_wi, and the rate of loss of tungsten atoms, ω_wa, are related by the equation

$$\omega_\mathrm{wi}=-\omega_\mathrm{wa}=K_\mathrm{iw}n_\mathrm{e}n_\mathrm{wa}-K_\mathrm{rw}n_\mathrm{e}^2n_\mathrm{wi}, \tag{11}$$

where K_iw is the rate coefficient for electron impact ionization, K_rw is the rate coefficient for the backward reaction of recombination, and n_wa and n_wi are respectively the number densities of tungsten atoms and ions. The notations '*wa*' and '*wi*' used here and below stand for tungsten atoms and tungsten ions, respectively.

The transport equations of tungsten atoms and ions diffusing in the mixture of electrons, argon atoms and argon ions are written based on equation (6) considering binary diffusion coefficients of tungsten species with the species of the background plasma. The derivation is similar to that for n_i given in appendix. Binary terms including tungsten atoms and ions are dropped.

Details on cross sections, rate coefficients and binary diffusion coefficients are given in appendix. Dimensionless number densities of tungsten atoms $\hat{n}_\mathrm{wa}$ and ions $\hat{n}_\mathrm{wi}$ are introduced similarly as it was done in the case of argon ions.

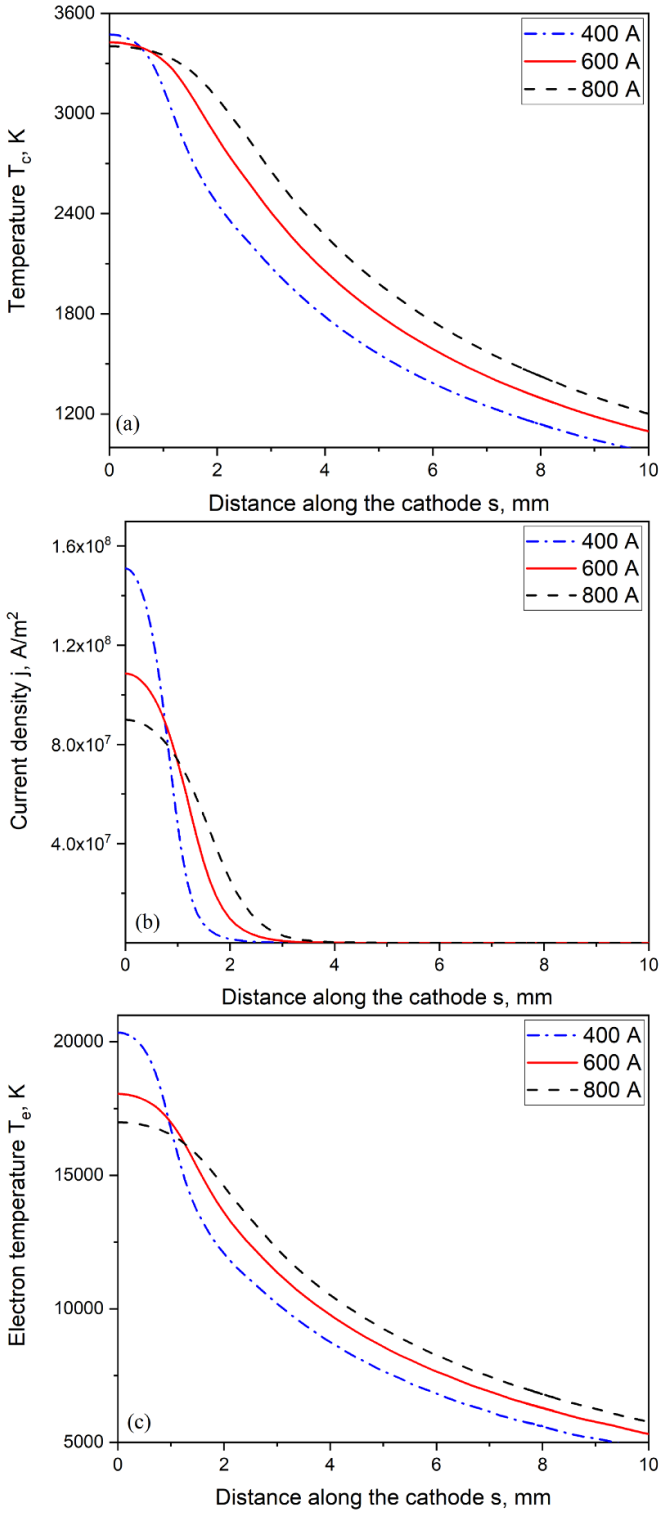

Figure 5. Computed values of the temperature T_c (a), the current density j (b), and the electron temperature T_e (c) on the cathode surface in the combined model of the plasma torch [8].

Appropriate boundary conditions to the transport equations of the tungsten atoms and ions are needed. At $x = L$, the 'zero gradient' boundary conditions $\frac{d\hat{n}_{wa}}{dx} = 0$ and $\frac{d\hat{n}_{wi}}{dx} = 0$ are adopted. At $x = 0$, the absorbing boundary condition for the tungsten ions $\hat{n}_{wi} = 0$ is used.

The boundary condition for the tungsten atoms needs particular attention. It can be derived implying the so called 'two-stream approximation' [4, 11–14]. In this approximation, the densities of particle fluxes moving from the boundary (J^+_{wa}) and to the boundary (J^-_{wa}) are determined. The net flux density is given as

$$J_{wa} = J^+_{wa} - J^-_{wa}. \tag{12}$$

In general, J^+_{wa} contains emitted and reflected particles, i.e.

$$J^+_{wa} = J_{vap} + rJ^-_{wa}, \tag{13}$$

with r denoting the reflection coefficient, and J_{vap} representing the density of the flux of evaporated tungsten atoms. Provided that r and J_{vap} are known, J^-_{wa} has to be expressed in terms of hydrodynamic parameters. One approximation [14] is to assume that the distribution of tungsten atoms is isotropic and Maxwellian so that

$$J^-_{wa} = n_{wa}\overline{V}_{th}/4, \tag{14}$$

where $\overline{V}_{th} = \sqrt{8k_B T_h/(\pi m_w)}$ is the average thermal velocity of tungsten atoms. This leads to a boundary condition relating the flux and the number density (the Robin type)

$$J_{wa} + (1-r)n_{wa}\frac{\overline{V}_{th}}{4} = J_{vap}. \tag{15}$$

Another form of the boundary condition can be derived assuming a 'half-Maxwellian' distribution and relating the fluxes J^+_{wa} and J^-_{wa} to the corresponding number densities n^+_{wa} and n^-_{wa} as [4]

$$J^{+,-}_{wa} = n^{+,-}_{wa}\frac{\overline{V}_{th}}{2}. \tag{16}$$

The total density at $x = 0$ is then expressed as

$$n_{wa} = \frac{2}{\overline{V}_{th}}(J^+_{wa} + J^-_{wa}). \tag{17}$$

Equations (12) and (17) yield

$$J^+_{wa} = (\frac{1}{2}n_{wa}\overline{V}_{th} + J_{wa})/2,$$
$$J^-_{wa} = (\frac{1}{2}n_{wa}\overline{V}_{th} - J_{wa})/2. \tag{18}$$

One replaces equations (18) into (13) to obtain the relation between the density of particle flux and number density of tungsten atoms at $x = 0$

$$J_{wa} + \frac{1-r}{1+r}n_{wa}\frac{\overline{V}_{th}}{2} = \frac{2}{1+r}J_{vap}. \tag{19}$$

Equation (19) provides another Robin type boundary condition to the equation for n_{wa}. In the case reflection is not taken into account ($r = 0$), it takes the form:

$$J_{wa} + n_{wa}\frac{\overline{V}_{th}}{2} = 2J_{vap}. \tag{20}$$

The conditions (15) and (20) have been known for a long time, e.g. equation (38) of [12], equation (2.1.12) of [15], equation (11) of [4], and equation (9) of [13]. A recent work by Benilov *et al* [14] discusses limiting cases, where the boundary condition (19) can lead to physically unrealistic results, e.g. when practically all released particles (electrons) are driven to the plasma and do not return to the cathode. Under the conditions in the present work, a physically unrealistic results may occur when J_{wa} reaches values larger than $n_{wa}\overline{V}_{th}/2$ (see equation (18)) so that J_{wa}^{-} (non-negative by definition) becomes negative. This can be the case of a strong sink of tungsten atoms near the cathode, e.g. due to ionization. The results presented below are obtained with equation (15) serving as a boundary condition at $x = 0$ for the equation concerning the transport of tungsten atoms and zero reflection ($r = 0$). The inapplicability of equation (20) in its form given by equation (19) as leading to physically unrealistic results is also demonstrated, which represents a new result for neutral atoms so far.

4. Transport of tungsten atoms and ions in the unified microarc model

Tungsten atoms and ions are included in the microarc plasma model and their transport occurs under conditions that are self-consistently computed for a given electric current density. The general features of the model of the microarc in atmospheric pressure argon are described in previous works (see e.g. [16]). The microarc model is adopted in the present work to account for the ionization and recombination of argon atoms and ions in the same way as this is done in the model of the ionization layer in section 3.1. This means that a singly charged atomic ion is considered with account for direct and stepwise ionization. The rate coefficients for ionization and recombination are the same as in the model of the ionization layer. In contrast to the model in section 3.1, the temperatures on the cathode T_c, the electron temperature T_e, and the temperature of heavy species T_h (argon atoms and ions) are not given input parameters but they are computed by solving the equations of energy conservation of the electrons and heavy species and the heat transfer in the tungsten cathode [16]. In the energy conservation equations, the same data for binary diffusion coefficients is used as in section 3.1. The electric field is obtained by solving the Poisson equation. Solid parts with a length of 10 mm are considered on both sides of the plasma region, which has a length of 1 mm. The model provides the number densities of argon species and electrons, their temperatures, and the electric field in the plasma region. If the temperature of the cathode is high enough, tungsten atoms are evaporated and released from the cathode. These atoms undergo ionization and recombination in collisions with electrons. The rate coefficients for these processes are the same as in section 3.1.

The boundary condition for argon ions on the electrodes are expressed in terms of fluxes [16]. The boundary conditions for tungsten species on the cathode are the same as in section 3.1. In particular, the boundary condition for tungsten atoms is given by equation (15) on the cathode. Absorbing boundary conditions are applied for tungsten atoms on the anode, and for tungsten ions on both the cathode and the anode. The temperature on the cathode end not in contact with the plasma is fixed at 300 K. For the sake of simplicity and since evaporation from the anode is not of interest in this work, its temperature is kept at 1000 K.

Table 1. Parameters at the center of the cathode for arc currents of 400, 600, and 800 A.

Current A	T_c, T_h K	T_e K	j 10^8 A m^{-2}
400	3473	20 342	1.50
600	3426	18 046	1.08
800	3402	16 981	0.89

5. Results and discussion

The transport of tungsten species in a background plasma in argon at atmospheric pressure is characterized by the models of the ionization layer and the model of the microarc plasma. The data that supports the results of this study are openly available in INPTDAT [17].

The studies carried out with the background plasma from the model of the ionization layer employ as input parameters findings obtained in the framework of the model combining the non-equilibrium boundary layer of the cathode and the equilibrium plasma in the plasma spray torch that were previously published [8]. These parameters as given in figure 5 show the distributions of (a) the temperature (T_c) and (b) the normal current density (j) on the cathode surface as well as (c) the electron temperature (T_e) for values of the electric current of 400 A, 600 A, and 800 A along the distance s, which is measured from the center of the cathode tip towards the cathode base. In [8], the boundary layer of the cathode is assumed to be very thin and is unresolved. In the model of the ionization layer (section 3.1), therefore, T_e represents an average value of the electron temperature, and the temperature of heavy species is constant and assumed equal to the cathode temperature, i.e. $T_h = T_c$. Notice the changes of the profiles of T_c, j, and T_e. With the increase of the total current at which the plasma torch is operated, the values at the center of the cathode ($s = 0$) decrease and the profiles become broader. This indicates a spreading of the arc attachment area with the increase of the arc current. While at a current of 400 A, 98.5% of the electric current is collected in the area closed by $s = 2$ mm, it is 92.7% at 600 A and 82.3% at 800 A. Nevertheless, the main arc attachment can be attributed to the rounded part of the cathode tip (see figure 2), where T_c (T_h), T_e and j do not deviate significantly from their values at the center of the cathode. These values are listed in table 1.

Figure 6 shows the computed number densities of neutral and charged particles in the ionization layer of the background plasma for input values of T_h, j, and T_e in table 1. Since the T_h-values lie within 70 K, the differences of n_a and n_i (n_e) result from the more significant difference in the values of T_e (see figure 5). The increase of n_i (n_e) and the decrease

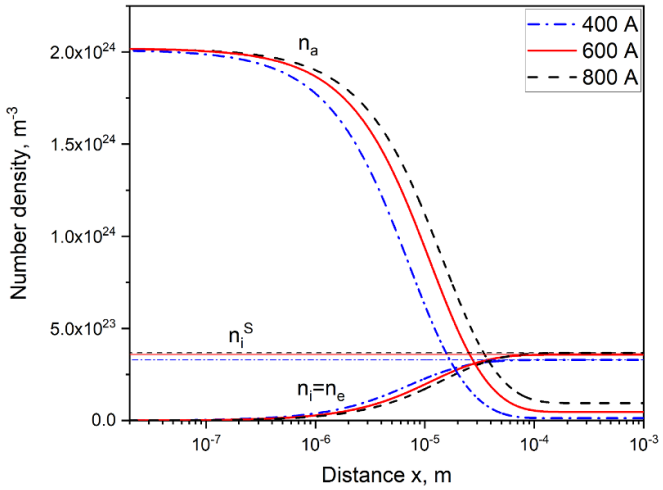

Figure 6. Number densities of neutral and charged species in the ionization layer of argon plasma at atmospheric pressure.

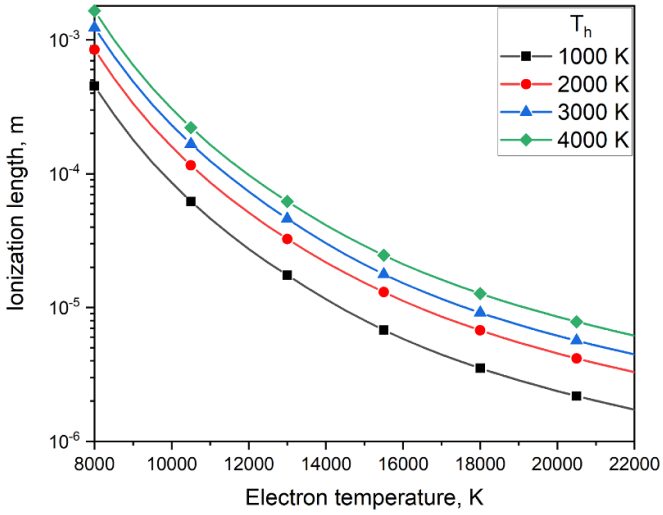

Figure 7. Ionization length for an argon plasma at atmospheric pressure.

of n_a occur at the shortest distance x in the case of an electric current of 400 A for which the electron temperature is the highest. The number densities of charged particles approach the values n_i^S corresponding to the ionization equilibrium at a distance of approximately 10^{-4} m. Notice that the ionization length shown in figure 7 as being computed after [18] amounts to $(5–20)\times10^{-6}$ m for T_h between 3000 and 4000 K and T_e between 16 000 and 20 000 K.

The number densities of tungsten particles along the distance x obtained with input parameters from table 1 are shown in figure 8. The equation for tungsten atoms is solved without and with account for a production of tungsten ions. The results for n_{wa} are marked as lines 1–3 and 4–6, respectively. Lines 7–9 represent the number density of tungsten ions n_{wi} for the three values of arc current. Notice the scales on the right-hand-side for lines 1–3 and on the left-hand-side for lines 4–9.

The number density n_{wa} is highest for the arc current of 400 A (line 1) and lowest for the arc current of 800 A

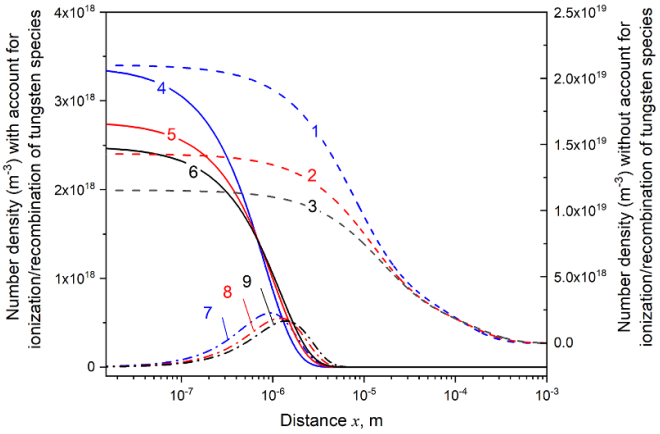

Figure 8. Number densities of tungsten atoms n_{wa} (1–6) and ions n_{wi} (7–9) along the distance x. Results for n_{wa} are obtained without (1–3) and with account of ionization (4–6) for electric currents of 400 A (1, 4, 7), 600 A (2, 5, 8), and 800 A (3, 6, 9).

(line 3). This results correlate with values of the cathode temperature T_c being the highest for 400 A and the lowest for 800 A. The equilibrium pressure p_v in equation (1) is strongly increasing with the temperature and overrules the temperature dependent denominator. Remarkably, the number density n_{wa} in all cases is vanishing towards the end of the ionization layer.

It was shown in [4] that in the case the equilibrium vapour pressure p_v is lower than the pressure of the undisturbed ambient gas and at large times, the number density of evaporated particles into a constant background of neutrals is constant (figure 2 in [4], line 6). That means that the net flux from the evaporating surface tends to zero. This result was obtained employing the Fick law in the time-dependent 1D equation of conservation of evaporated particles (equation (5) in [4]). We also obtain this result employing the Stefan–Maxwell equation (6) describing the diffusive transport of tungsten atoms into a homogeneous background of neutrals. The number density n_{wa} at the the cathode surface ($x=0$) tends then to the value $4J_{vap}/\overline{V}_{th}$ as it follows from equations (15) and (20) when J_{wa} tends to zero.

In the presence of a plasma background, the Stefan–Maxwell equation (6) written for n_{wa} does not reduce to the Fick law. According to equation (6), the diffusive velocity of tungsten atoms would be proportional to the gradient of their number density (Fick law) provided that the diffusive velocities of the argon atoms and ions were negligible. However, the significant sink of argon atoms due to their ionization leads to an appreciable diffusive flux, and the argon ions are driven by the strong electric field in the ionization layer (equation (10)) so that their diffusive velocity becomes very significant. The flux of tungsten atoms due to the density gradient is almost compensated by the flux caused by the argon ions. The friction between tungsten and argon atoms and between tungsten atoms and electrons are of minor importance. The fact that the Stefan–Maxwell equation does not conform to the Fick law in the case of diffusive transport of diluted particles has not been previously reported and is a new result.

The number density n_{wa} is reduced in the case of account for ionization/recombination processes between tungsten species and electrons. Notice that the case of no ionization considered here is an abstraction, which indicates the conditions established due to the backscattering of neutral tungsten atoms. In this case as discussed above, the net flux J_{wa} tends to zero and the number density n_{wa} amounts to $4J_{vap}/\overline{V}_{th}$. Due to the ionization, however, the net flux J_{wa} increases in absolute value and the number density n_{wa} decreases to fulfil equation (15). The value of n_{wa} at the cathode depends not only on the surface temperature of the cathode but also on the processes in the ionization layer.

The number density of tungsten ions n_{wi} reaches a maximum at a distance x between approximately $(1–2)\times10^{-6}$ m depending on the input parameters. The ionization occurs at a shorter distance at a current of 400 A (line 7), for which the electron temperature and number density are the highest. Notice that the n_{wa} and n_{wi} curves cross each other slightly beyond the positions of maximum n_{wi} values. The n_{wa} curves are vanishing at shorter distances than those of n_{wi}. Beyond the crossing point, the decrease of n_{wa} is steeper so that for $x\sim3\times10^{-6}$ m the ion number density n_{wi} significantly exceeds the atom number density n_{wa}. This means that the tungsten atoms become almost fully ionized at a distance of a few micrometers. However, the results further show that the number density of tungsten ions is also vanishing towards the edge of the ionization layer and there is no net flux of tungsten ions towards the equilibrium plasma. The ions are driven by the strong electric field in the ionization layer towards the cathode. As a result of these processes, there is no net flux of tungsten species leaving the ionization layer that can provide an estimate of the erosion rate of the cathode.

Before proceeding with the evaluation of the results of the transport of tungsten species within the framework of the unified microarc model (section 4), we briefly turn to the discussion on the boundary conditions given by equations (15) and (20). Figure 9 presents the values of J_{wa} along the distance x obtained for input parameters (T_h, j, and T_e) from table 1. The values of the flux of evaporated tungsten atoms J_{vap} computed after equation (1) are shown as solid bars. The J_{vap} value is highest at electric current of 400 A, for which the central value of the temperature on the cathode surface T_c is highest (see also figure 5). While the results obtained with equation (15) show values of J_{wa} towards the cathode lower than the corresponding J_{vap} value, those obtained when equation (20) is used, exceed the limiting J_{vap} value. Such results cannot be seen as physically realistic. Their origin is in the strength of the term describing the loss of tungsten atoms due to the net production of tungsten ions (equation (11)). A reduction of the ionization coefficient, e.g. by excluding the channel for stepwise ionization (see the appendix section), shows values below the limiting J_{vap} value. If ionization is not considered, both boundary conditions (15) and (20) deliver identical results. Therefore, we can conclude that the presence of the strong sink close to the cathode restricts the applicability of equation (20) as a boundary condition to the transport equation for neutral atoms released from the cathode surface. Although this issue was previously reported for electrons emitted from the cathode (see e.g. [14]), it is a new result for neutral atoms released from the cathode.

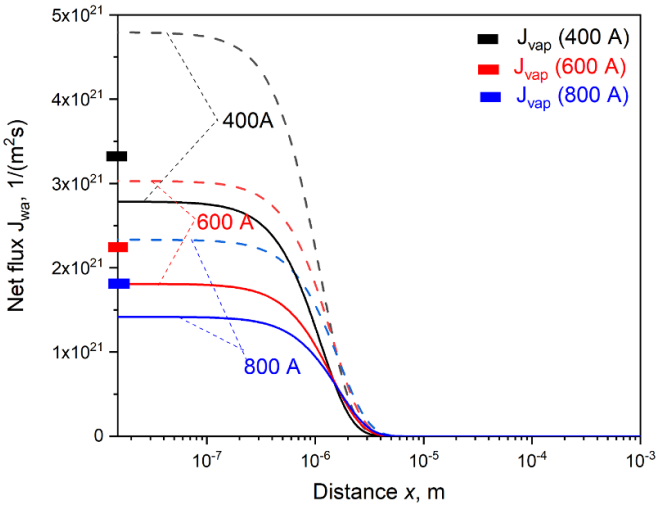

Figure 9. The density of net fluxes J_{wa} of particles obtained with input data from table 1 and boundary conditions given by equation (15) (solid lines) and by equation (20) (dashed lines). The J_{vap} values are indicated by markers on the left axis.

Thus, a description of the transport of tungsten species within only the ionization layer of atmospheric pressure argon plasma cannot provide the mechanism of removal of the species from the edge of the ionization layer. The evaporated tungsten atoms are almost fully ionized in a distance of a few micrometers from the cathode. The ions are driven back to the cathode by the electric filed. Flow velocities of several 100 m s^{-1} within a distance of 0.5 mm from the center of the cathode have been predicted by the combined model [8]. However, even if convection is taken into account (e.g. by introducing the material derivative $d/dt=\mathbf{v}\cdot\nabla$ into the stationary species equations), the net flux of tungsten ions tends to vanish.

Figure 10 shows the computed parameters of the microarc plasma in atmospheric pressure argon at a current density of 10^8 A m^{-2} along the distance x between the cathode ($x=0$) and the anode ($x=1$ mm): (a) the temperatures of electrons (T_e) and heavy particles (T_h); (b) the number densities of argon atoms (n_a) and ions (n_i), and electrons (n_e); (c) the modulus of the electric field. In contrast to the above considerations, the regions of space charge adjacent to the electrodes are resolved. In the log-scales of figures 10(a) and(b) the spatial extent of the cathode space charge sheath is well pronounced. While T_e does not vary that much and remains about 20 000 K for $x<10^{-4}$ m, T_h progressively increases starting with a value of about 4400 K on the cathode surface until it approaches T_e. The electric field (figure 10(c)) undergoes a reversal in the vicinity of the anode. A reversal of the electric field in the vicinity of the anode has been previously reported for arcs in atmospheric pressure argon and a length of several millimeters [19, 20] as well as in microarcs [16]. The accepted understanding is that the field reversal limits the electron flux to the anode in order to ensure that current continuity is preserved [21].

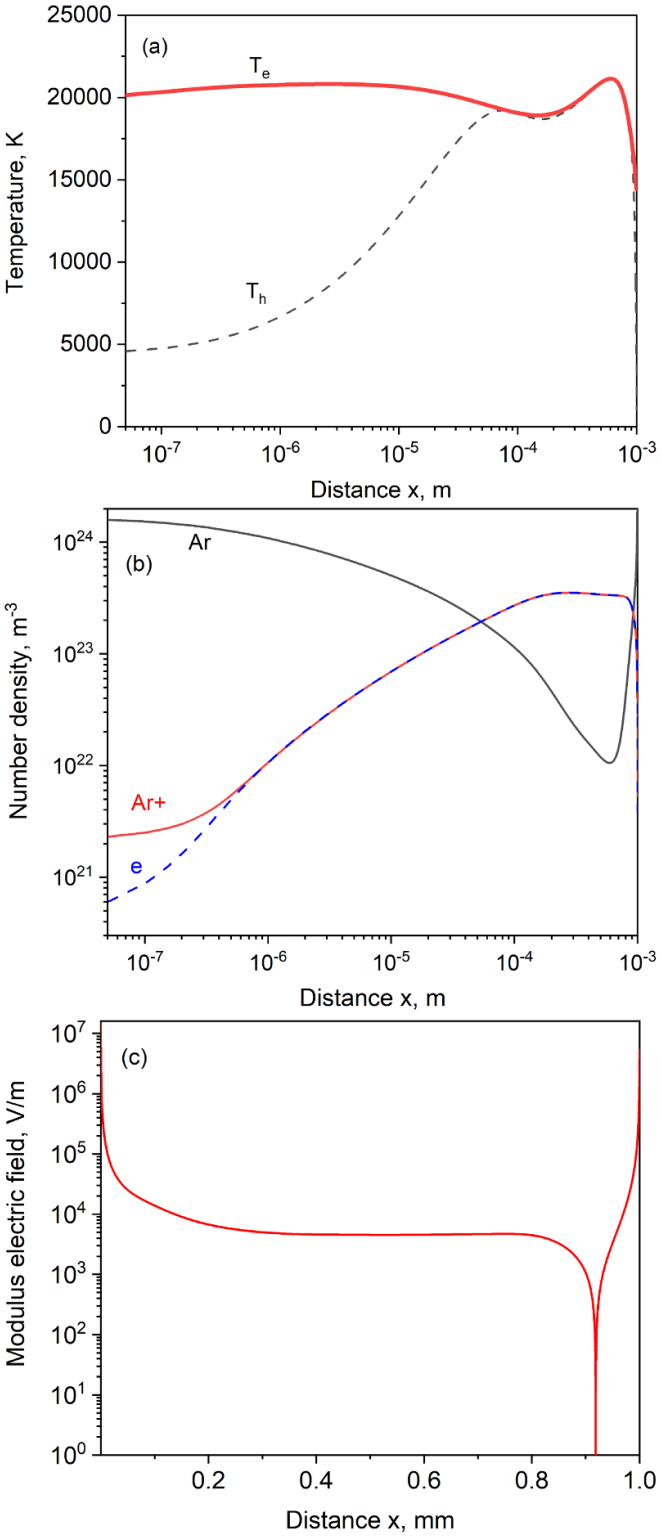

Figure 10. Parameters of the microarc plasma in atmospheric pressure argon at a current density of 10^8 A m^{-2}.

The distributions of the number densities of tungsten atoms and ions along the distance x are shown in figure 11. Similarly to the results with the model of the ionization layer discussed above, tungsten atoms released from the cathode are ionized within a distance of a few micrometers. Towards the

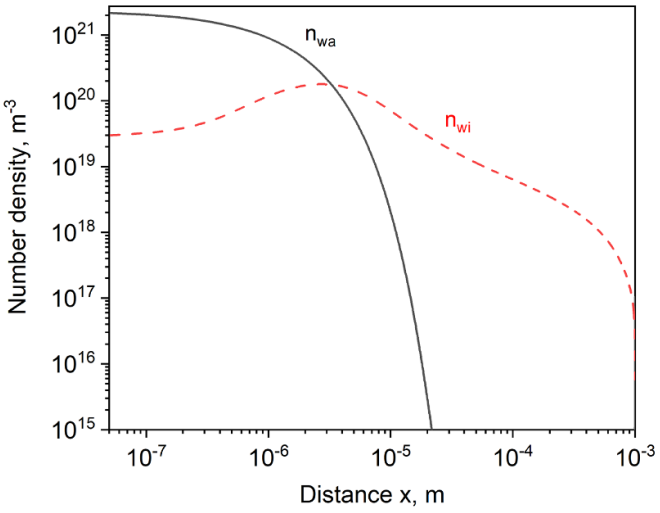

Figure 11. Number densities of tungsten atoms and ions at a current density of 10^8 A m^{-2}.

end of the ionization layer and the region of thermal equilibrium ($T_e = T_h$), the number density n_{wi} is decreasing to vanish at the anode. Notice that although the current density of 10^8 A m^{-2} is close to the values in table 1, the temperature on the cathode from the microarc model is higher and leads to a higher n_{wa} value. An adjustment of the temperature e.g. by changing the length of the cathode or by a setting of another value of the temperature at the cathode end, which is not in contact with the plasma, was not done. We are chasing a mechanism of removal of cathode material rather than providing a full agreement with experimental data.

In addition, the effect of convection is studied. Figure 12 shows results obtained without convection ($v = 0$) and a flow velocity of 100 and 200 m s^{-1}. These values of the convective velocity should be considered as average values. In reality, the flow velocity would be zero at the cathode and would increase along the distance x to become again zero at the anode. Notice that depending on the working conditions in the plasma spray torch, the axial fluid velocity predicted by means of the magneto-hydrodynamic model in [8] can reach values of several 100 m s^{-1} within a distance of 0.5 mm from the center of the cathode. The values of 100 and 200 m s^{-1} are used in order to indicate the role of the convection. The field reversal (figure 12(a)) occurs closer to the anode when convection is accounted for. A reversal of the diffusive velocity of tungsten ions ($v_{wi} = J_{wi}/n_{wi}$) is obtained even without account of convection (figure 12(b)). This reversal occurs at a distance of about 2×10^{-5} m, i.e. it is shifted with respect to the field reversal. An almost constant net density of particle flux of tungsten ions (figure 12(b)) is directed towards the anode as a result of the increasing diffusive velocity (figure 12(b)) and the decreasing number density of tungsten ions (figure 11). The reversal of the diffusive velocity is shifted closer to the anode if convection is accounted for. The larger the convective velocity the closer to the anode are the positions of the field and velocity reversals. The convection gives rise to the increase of the net density of particle flux of tungsten ions.

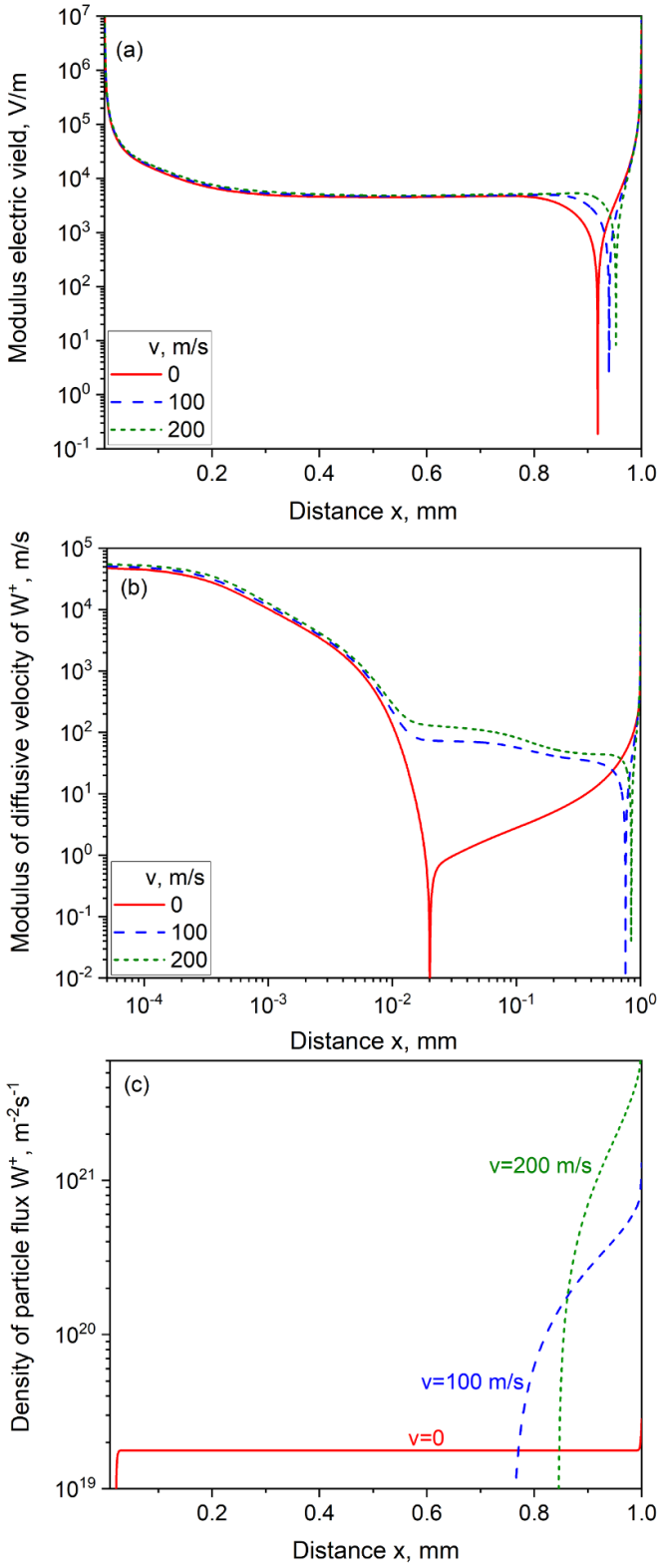

Figure 12. Effect of the convection on the electric field (a), the diffusive velocity (b) and density of particle flux (c) at a current density of 10^8 A m^{-2}.

The positive net density flux of tungsten ions (J_{wi}) towards the anode indicates that the field reversal provides a mechanism of removal of tungsten species although the anode can be seen as staying far away from the ionization layer of the cathode. Under conditions with temperature of the cathode below the boiling point, the transport of tungsten species is dominated by diffusion. The absorbing boundary condition provided by the anode is important to the diffusion into the plasma bulk. The flux J_{wi} allows us to estimate the mass loss of the cathode under the given conditions. Let us consider the area of a circle with a radius of 1 mm like the extent of the attachment area with a current density of about 10^8 A m^{-2} for arc currents of 600 and 800 A in figure 5(b). Then, the erosion rate is computed as the product of the area, the mass of the tungsten ions m_w, and the flux J_{wi}. With the values of J_{wi} of respectively 2×10^{19}, 7×10^{20}, and 5×10^{21} m^{-2}s^{-1} (see figure 12(c) for the cases 0, 100, and 200 m s^{-1}, respectively), the erosion rate amounts to 1.9×10^{-8}, 6.7×10^{-7}, and 4.8×10^{6} g s^{-1}. The mass loss of the cathode for one hour would amount to respectively, 0.07, 2.4, and 17.3 mg. In particular, the value of 2.4 mg corresponding to the case of an average convective velocity of 100 m s^{-1} matches the experimental values of (0.7–0.8) mg at 600 A and (2.2–3.1) mg at 800 A that are reported in section 2.

In the model of the ionization layer, the values of T_e, $T_h = T_c$, and j are used as input parameters. These values are obtained in the model of the plasma spray torch [8], in which the equilibrium plasma is coupled to the non-equilibrium boundary layer of the cathode. The latter is one-dimensional in direction perpendicular to the cathode surface, i.e. the one-dimensional model is applied to every grid node of the two-dimensional cathode surface. The values of T_e, $T_h = T_c$, and j (shown in figure 5) are obtained for a given total current (the integral of j over the cathode surface). The one-dimensional model of the ionization layer considered in the present work can be and it has been applied to every grid node on the cathode surface. The results corresponding to the center of the cathode have been only shown. However, no removal of tungsten species toward the plasma bulk has been obtained in all parametric studies. The one-dimensional model of the microarc computes the plasma parameters and the temperature on the cathode for a given value of the current density [16]. This feature is, however, of no relevance with respect to the mechanism of removal. The important difference between the two models is the presence of the anode in the model of microarc. The anode provides a sink of tungsten species and a reversal of the electric field, which enables that tungsten ions can be driven towards the anode and not all tungsten ions return to the cathode.

The transport of tungsten species considered with the model of the microarc argon plasma provides a mechanism of removal of tungsten ions from the ionization layer of the cathode towards the equilibrium plasma. This mechanism is fortified by a flow convection. It should be noticed that the one-dimensional model of the microarc was employed in order to indicate a probable mechanism of removal of tungsten species beyond the edge of the ionization layer of the cathode. The one-dimensional consideration implies a spatial variation of the plasma parameters in the direction x only. A two-dimensional description with the account for the shape of the cathode and magneto-hydrodynamic effects could affect the transport of tungsten species due to the spatial variation of the electric current density, the plasma parameters and

the electrode temperature. Apparently, the one-dimensional consideration of the microarc plasma differs from the realistic structure of the arc in the plasma spray torch. Nevertheless, it shows that the evaluation of the cathode erosion cannot be done by a model considering only the ionization layer, and indicates values of a mass loss of the cathode that are in a reasonable agreement with experimental findings. The question arises how the mass loss can be evaluated in multi-dimensional models based on the assumption of thermodynamic equilibrium in the arc plasma, where a reversal of the electric field does not usually occur. Non-equilibrium arc models, in which the ionization layers of the electrodes are resolved [20], should be capable of predicting the erosion rate of tungsten cathodes at the expense of higher computational efforts.

6. Conclusion

Experiments have indicated a mass loss of cathode material of about (0.7–0.8) mg at 600 A and (2.2–3.1) mg at 800 A per 1 h of operation of a plasma spray torch Oerlikon Metco F4MB-XL in atmopsheric pressure argon. These values are much lower than those obtained with the use of the Langmuir formula. The transport of tungsten atoms released from the cathode due to evaporation has been studied in relation to the evaluation of the erosion rate. The transport of tungsten species has been studied by means of two models. The results can be summarized as follows.

First, vaporization of a tungsten cathode separated from an equilibrium plasma by a non-equilibrium near-cathode layer was considered. Solutions have been obtained with input parameters known from a self-consistent modelling of the plasma spray torch reported previously. It has been shown that the tungsten atoms undergo an almost fully ionization in the background argon plasma within a distance of a few micrometers from the cathode. The number density of tungsten atoms vanishes due to the full ionization. This behaviour differs from that in a homogeneous neutral gas, it indicates that the Stefan–Maxwell equation cannot always be reduced to the Fick law, and represents a result never reported before for neutral atoms released from the cathode. The tungsten ions are driven back to the cathode by the electric field, which results in a vanishing net flux of tungsten species towards the plasma. Thus, a treatment of vaporization of a tungsten cathode separated from an equilibrium plasma by a non-equilibrium near-cathode layer does not provide a mechanism of removal of tungsten from the near-cathode region and hence of cathode erosion, even if a convective transport is taken into account. In other words, the cathode erosion is governed by processes not only in the near-cathode region but, mostly, in the arc bulk; a conclusion potentially important for practice.

The results obtained further show that a strong sink of tungsten atoms appears near the cathode surface due to the ionization of the evaporated atoms. In the case of no ionization sink, the gradient of the number density of tungsten atoms is small, and the net density of particle flux is small. The ionization sink causes an increase of the absolute value of the net density of particle flux of tungsten atoms of about two orders of magnitude compared with the values obtained without the account of ionization. This effect has given rise to study the appropriateness of the boundary condition for tungsten atoms on the cathode. It has been shown that under the circumstances of the physical problem the boundary condition given by equation (15) is preferable over that in equation (20) since it avoids the increase of the density of net particle flux beyond the limiting value of the Langmuir formula. This is a new result as far as atoms are concerned.

Second, a unified model of microarcs has been employed, which resolves the entire region with a length of 1 mm separating the cathode and the anode. In this model, the temperatures of the cathode, heavy particles and electrons are computed along with the number densities of the plasma constituents for the current density of $10^8\,\mathrm{A\,m^{-2}}$, which corresponds to the value at the center of the cathode for operation with arc current of 600 and 800 A. Like in the model of the ionization layer only, the evaporated tungsten atoms become almost fully ionized within a distance of a few micrometers from the cathode. However, the presence of the anode provides a mechanism of removal of tungsten ions from the ionization layer of the cathode. This mechanism is attributed to the reversal of the electric field. The net flux of tungsten ions is then directed to the anode and is fortified by convection. Estimates of the mass loss of the cathode show values that are in a reasonable agreement with the experimental findings.

Data availability statement

The data that support the findings of this study are openly available at the following URL/DOI: 10.34711/INPTDAT.512 [17].

Acknowledgments

This work was funded by the European Union and the Federal State of Germany Mecklenburg-Western Pomerania (Project Number TBI-V-1-321-VBW-112). The technical support provided by Daniel Köpp during the experiments is greatly acknowledged. The work at Universidade da Madeira was supported by FCT—Fundação para a Ciência e a Tecnologia of Portugal under Project UIDP/50010/2020 and by European Regional Development Fundthrough the Operational Program of the Autonomous Region of Madeira 2014-2020 under Project PlasMa-M1420-01-0145-FEDER-000016.

Appendix

Cross section data and rate coefficients

According to [22], the rate coefficients for ionization of argon and tungsten atoms are computed accounting for direct and stepwise ionization channels, i.e K_i in equation (3) and K_iw in equation (11) are computed as

$$K_\mathrm{i,iw} = K^d_\mathrm{i,iw} + K^s_\mathrm{i,iw}. \tag{21}$$

The rate coefficients for direct ionization K^d are computed using the cross section for ionization of the ground state of the corresponding atom and assuming a Maxwellian velocity distribution function of the electrons in the ionization layer. For argon, the measured cross section by Rapp and Englander-Golden [23] is used. A summary of available cross section data can be found in [24, 25]. For tungsten, experimental data is not available so that computed data by Deutsch *et al* [26] is used.

The rate coefficients for stepwise ionization K^s are computed applying the modified diffusion approximation (MDA) [22]. According to the MDA, the ionization occurs as a result of the diffusion of bound electrons in the energy space of atomic levels. An energy level, at which the electron is at most, is considered as a bottleneck. For argon, this level is an effective level at an energy of 11.64 eV comprising the 4*s* levels of argon [27]. For tungsten, the effective level with an energy of 3.51 eV accounts for the levels $6p(7P^\circ,\ 5P^\circ)$ [27]. The partition function of the corresponding ion as dependent on the electron temperature is taken into account.

Binary diffusion coefficients

The binary diffusion coefficients are defined as [28]

$$D_{\rm kl} = \frac{3\pi}{16}\sqrt{\frac{2k_{\rm B}T_{\rm kl}}{\pi m_{\rm kl}}}\frac{1}{n\bar{Q}_{\rm kl}^{(1,1)}}, \tag{22}$$

where $T_{\rm kl}$ and $m_{\rm kl}$ denote respectively the reduced temperature and the reduced mass for species of type k and l given as $T_{\rm kl} = \frac{m_{\rm k}T_{\rm l}+m_{\rm l}T_{\rm k}}{m_{\rm k}+m_{\rm l}}$ and $m_{\rm kl} = \frac{m_{\rm k}m_{\rm l}}{m_{\rm k}+m_{\rm l}}$, and $\bar{Q}_{\rm kl}^{(1,1)}$ represent energy-averaged cross sections for momentum transfer.

For atom-atom interactions, $\bar{Q}_{\rm kl}^{(1,1)}$ are generally expressed as [28]

$$\bar{Q}_{\rm kl}^{(1,1)} \equiv \pi\sigma_{\rm kl}^2\,\Omega_{\rm kl}^{(i,j)*}. \tag{23}$$

Here, $\sigma_{\rm kl}$ is the distance between the centers of the two atoms and $\Omega_{\rm kl}^{(i,j)*}$ is the reduced Ω-integral. The parameters of the Lennard–Jones (12, 6) potentials [29] and empirical equations for the reduced Ω-integrals [30] are used to compute $\bar{Q}_{kl}^{(1,1)}$.

Atom-ion interactions Ar–Ar^+ and W–W^+ are governed by charge transfer cross sections [31] $\sigma_{cx} = \sigma_0[1 - a\ln(1/\varepsilon(eV))]^2$ with parameters σ_0 equal to 4.8×10^{-19} m^2 for argon and 17×10^{-19} m^2 for tungsten, and parameters a equal to 0.14 for argon and 0.1 for tungsten. The energy-averaged cross section is taken as twice the charge transfer cross section.

Atom-ion interactions W–Ar^+ and Ar–W^+ are governed by polarization interactions [32] with polarizability values of $68a_0^3$ for tungsten and $11.08a_0^3$ for argon [33] (a_0 is the Bohr radius). The correction factors $C_{\rm kl}$ in equation (6) are set to one for atom-ion interactions.

Electron-atom collisions are accounted with the cross sections for momentum transfer [34, 35]. The evaluation of the correction coefficients $C_{\rm ae}$ and $C_{\rm we}$ follows the that in [36].

The ion-electron interactions are described following [28] so that

$$\bar{Q}_{\rm ie}^{(1,1)} = 2\pi\left(\frac{e^2}{4\pi\varepsilon_0}\right)^2\frac{1}{2(k_{\rm B}T_{\rm e})^2}\frac{\ln(4z_0^2+1)}{4}, \tag{24}$$

where e is the elementary charge, ε_0 is the dielectric permittivity of free space, $z_0 = 2k_{\rm B}T_{\rm e}(\frac{e^2}{4\pi\varepsilon_0})^{-1}\lambda_{\rm D}$ and $\lambda_{\rm D}$ is the Debay length. The ion–ion interactions are treated in the same way. The correction coefficients are set to 0.5076.

Transformation of the transport species equations

For tungsten atoms, one can write the equation

$$\begin{aligned}\frac{dn_{\rm wa}}{dx} = &-\left(n_a\frac{C_{\rm wa,a}}{nD_{\rm wa,a}} + n_i\frac{C_{\rm wa,i}}{nD_{\rm wa,i}} + n_e\frac{T_{\rm e}}{T_{\rm h}}\frac{C_{\rm wa,e}}{nD_{\rm wa,e}}\right)J_{\rm wa}\\ &+ n_{\rm wa}\left(\frac{T_{\rm e}}{T_{\rm h}}\frac{C_{\rm wa,e}}{nD_{\rm wa,e}} + \frac{C_{\rm wa,i}}{nD_{\rm wa,i}} - \frac{C_{\rm wa,a}}{nD_{\rm wa,a}}\right)J_{\rm i}\\ &- n_{\rm wa}\frac{T_{\rm e}}{T_{\rm h}}\frac{C_{\rm wa,e}}{nD_{\rm wa,e}}j/e.\end{aligned} \tag{25}$$

The density flux of tungsten atoms can be expressed as

$$J_{\rm wa} = -\frac{1}{d_{\rm w}}\frac{dn_{\rm wa}}{dx} + \frac{n_{\rm wa}}{d_{\rm w}}\left[g_{\rm w}J_{\rm i} - \frac{T_{\rm e}}{T_{\rm h}}\frac{C_{\rm wa,e}}{nD_{\rm wa,e}}j/e\right], \tag{26}$$

where

$$d_{\rm w} = n_{\rm i}\frac{C_{\rm wa,i}}{nD_{\rm wa,i}} + n_{\rm a}\frac{C_{\rm wa,a}}{nD_{\rm wa,a}} + n_{\rm e}\frac{T_{\rm e}}{T_{\rm h}}\frac{C_{\rm wa,e}}{nD_{\rm wa,e}},$$

and

$$g_{\rm w} = \frac{C_{\rm wa,i}}{nD_{\rm wa,i}} - \frac{C_{\rm wa,a}}{nD_{\rm wa,a}} + \frac{T_{\rm e}}{T_{\rm h}}\frac{C_{\rm wa,e}}{nD_{\rm wa,e}}.$$

$J_{\rm wa}$ can be replaced in equation (2) to obtain an equation similar to equation (7). The procedure to obtain the equation for $n_{\rm wi}$ follows that for $n_{\rm wa}$.

ORCID iDs

M Baeva https://orcid.org/0000-0003-3305-2870
M S Benilov https://orcid.org/0000-0001-9059-1948
T Zhu https://orcid.org/0000-0002-9419-4170
T Kewitz https://orcid.org/0000-0002-8252-7265

References

[1] Nemchinsky V 2012 Cathode erosion in a high-pressure high-current arc: calculations for tungsten cathode in a free-burning argon arc *J. Phys. D: Appl. Phys.* **45** 135201
[2] Nemchinsky V 1996 Life time of a refractory cathode doped with a work-function-lowering dopant *J. Phys. D: Appl. Phys.* **29** 2417–22
[3] Konishi K, Tanaka M, Shigeta M and Ishida K 2017 Numerical analysis of dynamic behavior of additives in electrode during TIG welding process *Q. J. Japan Weld. Soc.* **35** 73–84

[4] Benilov M S, Jacobson S, Kaddani A and Zahrai S 2001 Vaporization of a solid surface in an ambient gas *J. Phys. D: Appl. Phys.* **34** 1993–9

[5] Ortega D, Sillero Martin J A, Munoz-Serrano E and Casado E 2009 Simulation of the atomic and ionic densities in the ionization layer of a plasma arc with a binary cathode *J. Phys. D: Appl. Phys.* **42** 085202

[6] Almeida R M S , Benilov M S and Naidis G V 2000 Simulation of the layer of non-equilibrium ionization in a high-pressure argon plasma with multiply-charged ions *J. Phys. D: Appl. Phys.* **33** 960–7

[7] F4MB-XL BRO-0006.6 2015 Atmospheric plasma spray solutions

[8] Baeva M, Zhu T, Kewitz T, Testrich H and Foest R 2021 Self-consistent cathode-plasma coupling and role of the fluid flow approach in torch modelling *J. Therm. Spray Technol.* **30** 1737–50

[9] Plansee SE 2022 Plasma electrodes and nozzles. Molybdenum spray wire (available at: www.plansee.com)

[10] Zhdanov V M 2002 *Transport Phenomena in Multicomponent Plasma* (London: Taylor and Francis)

[11] McDaniel E W 1964 *Collision Phenomena in Ionized Gases* (New York: Willey)

[12] Sajben M 1970 Boundary conditions for adsorbing-emitting electrodes in contact with seeded, dense plasmas *AIAA J.* **8** 400–6

[13] Gorin V V, Kudryavtsev A A, Yao J, Yuan C and Zhou Z 2020 Boundary conditions for drift-diffusion equations in gas-discharge plasmas *Phys. Plasmas* **27** 013505

[14] Benilov M S, Almeida P G C, Ferreira N G C , Almeida R M S and Naidis G V 2021 A practical guide to modeling low-current quasi-stationary gas discharges: eigenvalue, stationary and time-dependent solvers *J. Appl. Phys.* **130** 121101

[15] Stakhanov I P and Cherkovets V E 1985 *Physics of a Thermionic Converter* (Moscow: Energoatomizdat)

[16] Baeva M, Loffhagen D and Uhrlandt D 2019 Unified non-equilibrium modelling of tungsten-inert gas microarcs in atmospheric pressure argon *Plasma Chem. Plasma Process.* **39** 1359–78

[17] Baeva M, Benilov M S, Zhu T, Testrich H, Kewitz T and Foest R Modelling and experimental evidence of the cathode erosion in a plasma spray torch–dataset 2022 *INPTDAT* (available at: http://doi.org/10.34711/INPTDAT.512)

[18] Benilov M S 1999 Analysis of ionization non-equilibrium in the near-cathode region of atmospheric-pressure arcs *J. Phys. D: Appl. Phys.* **32** 257–62

[19] Yang G and Heberlein J 2007 Anode attachment modes and their formation in a high intensity argon arc *Plasma Sources Sci. Technol.* **16** 529–42

[20] Baeva M, Benilov M S, Almeida N A and Uhrlandt D 2016 Novel non-equilibrium modelling of a DC electric arc in argon *J. Phys. D: Appl. Phys.* **49** 245205

[21] Mentel J and Heberlein J 2010 The anode region of low current arcs in high intensity discharge lamps *J. Phys. D: Appl. Phys.* **43** 023002

[22] Biberman L M, Vorob'ev V S and Yakubov I T 1987 *Kinetics of Nonequilibrium Low-Temperature Plasma* (New York: Plenum)

[23] Rapp D and Englander-Golden P 1965 Total cross sections for ionization and attachment in gases by electron impact. I. Positive ionization *J. Chem. Phys.* **43** 1464–79

[24] Yanguas-Gil A, Cotrini J and Alves L 2005 An update of argon inelastic cross sections for plasma discharges *J. Phys. D: Appl. Phys.* **38** 1588–98

[25] Alves L L 2014 The IST-LISBON database on LXCat *J. Phys.: Conf. Ser.* **565** 012007

[26] Deutsch H, Hilpert K, Becker K , Probst M and Maerk T D 2001 Calculated absolute electron-impact ionization cross section for AlO, Al_2O and WO_x (x=1–3) *J. Appl. Phys.* **89** 1915–21

[27] Kramida A, Ralchenko Y and Reader J (NIST ASD Team) 2019 NIST Atomic Spectra Database (Version 5.7.1)

[28] Ferziger J H and Kaper H G 1972 *Mathematical Theory of Transport Processes in Gases* (Amsterdam: North-Holland)

[29] Zhen S and Davies G J 1983 Lennards-Jones n-m potential energy parameters *Phys. Status Solidi(a)* **78** 595–605

[30] Neufeld P D, Jamzen A R and Aziz R A 1972 Empirical equations to calculate 16 of the transport collision integrals $\Omega^{(l,s*)}$ for the Lennard-Jones (12–6) potential *J. Chem. Phys.* **57** 1100–2

[31] Anders A 1990 *A Formulary for Plasma Physics* (Berlin: Akademie-Verlag)

[32] Kihara T, Taylor M H and Hirschfelder J O 1960 Transport properties for gases assuming inverse power intermolecular potentials *Phys. Fluids* **3** 715–20

[33] Schwerdtfeger P and Nagle J K 2019 2018 Table of static dipole polarizabilities of the neutral elements in the periodic table *Mol. Phys.* **117** 1200–25

[34] Hayashi M 2003 Bibliography of electron and photon cross sections with atoms and molecules published in the 20th century *NIFS-DATA-72 Report, Argon*

[35] Blanco F, da Silva F F, Lim ao-Vieira P and Garcia G 2017 Electron scattering cross section data for tungsten and beryllium atoms from 0.1 to 5000 eV *Mol. Phys.* **26** 085004

[36] Almeida N A, Benilov M S and Naidis G V 2008 Unified modelling of near-cathode plasma layers in high-pressure arc discharges *J. Phys. D: Appl. Phys.* **41** 245201